

FINAL REPORT

“Addressing Control Research Issues Leading to Piloted Simulations in Support of the IFCS F-15”

NASA Grant/Cooperative Agreement NCC4-159

by:

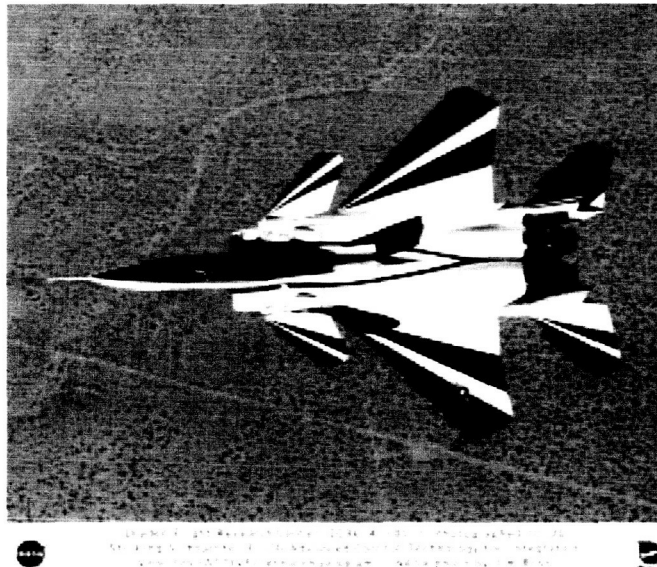
Marcello Napolitano, Professor, Principal Investigator
Mario Perhinschi, Assistant Professor, Co-Principal Investigator
Giampiero Campa, Research Assistant Professor
Brad Seanor, Research Assistant Professor

Department of Mechanical and Aerospace Engineering
West Virginia University, Morgantown, WV 26506/6106

submitted to:

John Burken, Chief Engineer, Control and Dynamics Branch
NASA Dryden Flight Research Center
MS 4840D, PO BOX 273
Edwards, CA 93523-0273
Tel. (661) 2763726; E-mail: John.Burken@mail.dfrc.nasa.gov

June 2004



Abstract

This report summarizes the research effort by a team of researchers at West Virginia University in support of the NASA Intelligent Flight Control System (IFCS) F-15 program. In particular, WVU researchers assisted NASA Dryden researchers in the following technical tasks leading to piloted simulation of the ‘*Gen_2*’ IFCS control laws.

Task #1- Performance comparison of different neural network (NN) augmentation for the Dynamic Inversion (DI) -based VCAS ‘*Gen_2*’ control laws.

Task #2- Development of safety monitor criteria for transition to research control laws with and without failure during flight test.

Task #3- Fine-tuning of the ‘*Gen_2*’ control laws for cross-coupling reduction at post-failure conditions.

Matlab/Simulink-based simulation codes were provided to the technical monitor on a regular basis throughout the duration of the project. Additional deliverables for the project were Power Point-based slides prepared for different project meetings.

This document provides a description of the methodology and discusses the general conclusions from the simulation results.

Table of Contents

Abstract	2
Table of Contents	3
List of Acronyms	4
1. Introduction	5
2. Performance of different neural network augmentation for the non-linear dynamic inversion (NLDI) - based control laws	6
2.1. Introduction	6
2.2. The Dynamic Inversion-Based Control Laws	6
2.3. The Extended Minimal Resource Allocating Networks Algorithm	7
2.4. The Single Hidden Layer Neural Network Algorithm	8
2.5. The Sigma-Pi Neural Network	9
2.6. Results of the Comparative Study	9
2.7. Conclusions	10
3. Safety monitor schemes for transition to research control laws	11
3.1 Introduction	11
3.2. Description of the “Safety Monitor” Scheme	11
3.2.1. Operation Modes	11
3.2.2. Abnormal Situations	12
3.2.3. Floating Limiter	13
3.2.4. Sub-scheme #1 (SM#1)	14
3.2.5. Sub-scheme #2 (SM#2)	14
3.3. Description of the IFCS F-15 Simulation Code	14
3.4. Description of the Interface Between the SM Scheme and the WVU IFCS F-15 Simulator	15
3.5. Simulation Results for Different Scenarios	15
3.6. Simplified SM scheme	16
3.6.1. Simplified floating limiter	16
3.6.2. Range Limiter	17
3.6.3. Persistence Counter	17
3.6.4 Reduced number of parameters monitored	17
3.6.5. Testing of the simplified scheme	18
3.7. Conclusions	18
4. Modifications to Remove Cross-Coupling Issues on the IFCS F-15 Control Laws	19
4.1. Introduction	19
4.2. Cross-coupling parameters	19
4.3. Simulation results	19
4.3.1. Test Case #1	19
4.3.2. Test Case #2	20
4.3.3. Test Case #3	20
4.4 Conclusions	20
References	21
Tables & Figures	23

List of Acronyms

BFC	Basic Flight Computer
CCL	Conventional Control Laws
CCT	Cross-Coupling Terms
DI	Dynamic Inversion
EMRAN	Extended Minimal Resource Allocating Networks
FCS	Flight Control System
FDI	Failure Detection and Identification
FL	Floating Limiter
FM	Simulated Failure Mode
<i>Gen_2</i>	2 nd generation
IFCS	Intelligent Flight Control System
NLDI	Non Linear Dynamic Inversion
NM	Nominal Mode
NN	Neural Network
PCH	Pseudo-Control Hedging
RCL	Research Control Laws
RFC	Research Flight Computer
RM	Research Mode
SHL	Single Hidden Layer
SM	Safety Monitor
SP	Sigma Pi
WVU	West Virginia University

1. Introduction

The contribution of the West Virginia University (WVU) research team to the NASA Intelligent Flight Control System (IFCS) 'Gen_2' F-15 project between 3/1/2003 and 2/29/2004 includes the following:

1- Comparison of the performance of different neural network (NN) augmentation for the Dynamic Inversion (DI) - based control laws.

An extensive simulation study has been performed¹ focused on comparing the performance of three different neural augmentations for the dynamic inversion-based control laws used for fault tolerant purposes on the NASA IFCS F-15 aircraft with the 'Gen_2' research activities. In particular, the performance of the Extended Minimal Resource Allocating Networks (EMRAN) algorithm, the Single Hidden Layer (SHL) neural network, and the Sigma Pi (SP) neural network have been compared. The comparison has been conducted in terms of 'ad-hoc' parameters relative to the tracking of desirable dynamic responses following the injection of simulated failures on the actuators of the right stabilator and the left canard of the NASA F-15 aircraft. The simulation results have shown that all three neural networks have promising performance with the Extended Minimal Resource Allocating Networks algorithm slightly outperforming the other algorithms.

2- Development of safety monitor criteria for transition to research control laws with and without failure during flight test.

Specific parameters have been identified and criteria have been defined for the development of a Safety Monitor (SM) scheme for safe transition to research control laws with and without failure during flight test. A SM scheme has been developed and tested² at WVU allowing the flight control system to switch from "nominal" mode to "research" mode. Within the "research" mode the research objectives are to investigate the performance of a neural network-based set of control laws for fault tolerant purposes. In a typical research aircraft, the "conventional" control laws are implemented on the "basic" flight computer (SC3) while research control laws – designed to provide fault tolerance capabilities - are housed on a research computer (ARTS2). Therefore, a safety logic scheme is needed to ensure a safe transition from the conventional to the research control laws at nominal conditions, as well as from the research control laws at nominal conditions to the research control laws with "simulated" failures on specific control surfaces. The SM scheme along with its logic for the different transitions have been designed using information relative to different parameters, such as flight conditions and controller-related performance criteria. The testing of the SM was performed through a customized interface with a detailed Simulink-based flight simulation code developed at WVU for the NASA IFCS-15 aircraft³. Different levels of complexity of the SM scheme have been considered; the trade-offs between complexity and efficiency have been identified.

3- Enhancement of the control laws to provide improved cross-coupling reduction at post-failure conditions.

Pilot evaluation during ground simulator tests showed undesirable levels of cross coupling at post failure conditions. The introduction of 'coupling terms' in the cost function of the NNs has been investigated as a possible solution. Particularly, products of the angular rates and angular rate cross correlations have been considered as possible coupling terms to be added to the cost function. Simulation results showed a sensible decrease of the cross-coupling.

2. Performance of different neural network augmentation for the non-linear dynamic inversion (NLDI) - based control laws

2.1. Introduction

The main goal of the NASA IFCS F-15 program⁵ is to develop and evaluate in flight control schemes allowing the pilot to cope with the occurrence of a primary control surface failure. The control laws considered here are based on a NLDI scheme augmented with a NN to compensate inversion errors and changes in aircraft dynamics due to damage or failure of primary control surfaces. The performance of three different NNs is investigated starting from a well-known architecture⁶⁻¹⁰. The three NNs considered are: the Extended Minimal Resource Allocating Networks¹¹ (EMRAN) algorithm, the Single Hidden Layer⁸ (SHL) NN, and the SigmaPi¹². Their performance is compared in different simulations involving nominal flight conditions, as well as stabilator and canard failures.

2.2. The Dynamic Inversion-Based Control Laws

The general scheme is based on an adaptive neural controller canceling the errors associated with the dynamic inversion of the model. This control strategy⁶⁻⁸ has been selected to provide consistent handling qualities without requiring the level of computational effort associated with gain-scheduling and/or system identification. In addition, desired handling qualities are achieved with '*ad hoc*' reference models.

Flight commands are generated by the pilot through longitudinal and lateral stick ($\delta_{lonstick}$, $\delta_{latstick}$) and pedals ($\delta_{dirpedal}$). These displacement commands are converted⁶⁻¹⁰ into corresponding roll, pitch, and yaw rate commands (p_{com} , q_{com} , r_{com}). The reference model provides filtered rate commands (p_{ref} , q_{ref} , r_{ref}) and acceleration commands (\dot{p}_{ref} , \dot{q}_{ref} , \dot{r}_{ref}) using first order roll rate and second order pitch and yaw rate transfer functions.

The inputs to dynamic inversion (\dot{p}_c , \dot{q}_c , \dot{r}_c) are computed using the expression:

$$\begin{bmatrix} \dot{p}_c \\ \dot{q}_c \\ \dot{r}_c \end{bmatrix} = \begin{bmatrix} U_p \\ U_q \\ U_r \end{bmatrix} - \begin{bmatrix} U_{pad} \\ U_{qad} \\ U_{rad} \end{bmatrix} \quad (1)$$

where (U_{pad} , U_{qad} , U_{rad}) are augmentation commands generated by adaptive NNs in order to compensate for the estimated errors e_p , e_q , e_r from the difference between reference and plant angular rates. Furthermore, the pseudo control acceleration commands (U_p , U_q , U_r) are computed with the following expressions:

$$U_p = \left(K_{p_p} + \frac{K_{i_p}}{s} \right) \cdot e_p + s \cdot p_{ref} \quad (2)$$

$$U_q = \left(K_{p_q} + \frac{K_{i_q}}{s} \right) \cdot e_q + s \cdot q_{ref} \quad (3)$$

$$U_r = \left(K_{p_r} + \frac{K_{i_r}}{s} \right) \cdot e_r + s \cdot r_{ref} \quad (4)$$

where K_p and K_i are, respectively, proportional and integral constants.

Dynamic inversion is then used to determine the necessary control surface deflections ($\delta_a, \delta_e, \delta_r$). Initially, control surface commands ($\delta_{a_{com}}, \delta_{e_{com}}, \delta_{r_{com}}$) are obtained with the following equation:

$$\begin{bmatrix} \delta_{a_{com}} \\ \delta_{e_{com}} \\ \delta_{r_{com}} \end{bmatrix} = B^{-1} \begin{bmatrix} \dot{p}_c - L_I \\ \dot{q}_c - M_I \\ \dot{r}_c - N_I \end{bmatrix} \quad (5)$$

where B is the state space system control matrix and the terms ($\dot{p}_c - L_I, \dot{q}_c - M_I, \dot{r}_c - N_I$) are the differences between input acceleration commands and actual plant acceleration contributions (L_I, M_I, N_I). These plant contributions are function of inertial and geometric characteristics, aerodynamic derivatives, angular rates, and aerodynamic angles. Finally, the control surface actual deflections are computed from $\delta_{a_{com}}, \delta_{e_{com}}, \delta_{r_{com}}$ in order to include the modeling of the actuator dynamics (first and second order transfer functions).

2.3. The Extended Minimal Resource Allocating Networks Algorithm

The first NN considered in this study is the *Extended Minimal Resource Allocating Networks*¹¹ (EMRAN) algorithm. The EMRAN algorithm is a more powerful version of the standard MRAN. The main architecture¹³ features growing and pruning mechanisms; moreover, the parameters are updated following a “winner takes it all” strategy. The extended algorithm allows only the parameters of the most activated neurons to be updated, while all the others are left unchanged. In other words, the algorithm allocates resources (neurons) in order to decrease the estimation error in regions of the state space where the mapping accuracy is poor. This strategy implies a significant reduction of the number of parameters to be updated on-line; thus, it is particularly suitable for on-line applications¹⁴.

For Gaussian basis functions the estimate is computed with the expression:

$$\hat{y}(x, \theta) = \sum_{i=1}^M w_i e^{\left(\frac{|x - \mu_i|^2}{2\sigma_i^2} \right)} \quad (6)$$

where x is the input vector, θ is the set of parameters to be tuned by the learning algorithm including the weight w , the gaussian center positions μ , and the variances σ . A new neuron is initiated if 3 distinct criteria are satisfied: the estimation error, the windowed estimation error, and the distance from the input to the nearest center must be larger than selected thresholds:

$$e_1(k) = y(k) - \hat{y}(k) > E_1 \quad (7)$$

$$\frac{1}{N} \sqrt{\sum_{i=1}^M e(k-i)} > E_2 \quad (8)$$

$$d_{BMU} = \min_{j=1, \dots, neu} (\|c(k) - x(k)\|) > E_3 \quad (9)$$

If this is the case, the center, variance, and weight of the new neuron at iteration k are given by, respectively:

$$\mu_{M+1}(k) = x(k) \quad (10)$$

$$\sigma_{M+1} = \lambda \inf_{j=1}^M \|x(k) - \mu_j(k)\| \quad (11)$$

$$w_{M+1}(k) = e(k) = y(k) - \hat{y}(k) \quad (12)$$

When one of the criteria is not met, the tuning parameters are updated using the relationship:

$$\theta(k+1) = \theta(k) - \eta \left. \frac{\partial \hat{y}(k)}{\partial \theta(k)} \right|_{(k)} \cdot e(k) \quad (13)$$

where $e(k)$ is the estimation error and η is the learning rate.

A combination of an ADALINE¹⁵ and an EMRAN network (A+EMRAN) working in parallel has been implemented on each of the three channels. This approach has been adopted to achieve good performance in the presence of large non-linearities without the computational burden on operation in areas without non-linearities.

2.4. The Single Hidden Layer Neural Network Algorithm

The second neural algorithm considered in this effort is the Single Hidden Layer^{6,7,8} (SHL) NN. The output of the network is given by the relationship:

$$y_i = \sum_{j=1}^m \left[w_{ij} \sigma \left(\sum_{k=1}^n v_{jk} x_k + \theta_{vj} \right) + \theta_{wi} \right], \quad i = 1, 2, \dots, p \quad (14)$$

where w_{ij} are the interconnection weights between the hidden layer and the output layer, v_{jk} are the interconnection weights between the input layer and the hidden layer, and θ_{vj} , θ_{wi} are bias terms. The activation potential a is used to compute the activation function of the form:

$$\sigma(\xi) = \frac{1}{1 + e^{-a\xi}} \quad (15)$$

Based on a Lyapunov analysis the weights updating laws are given by^{6,7,8}:

$$\begin{aligned} \dot{W} &= -\gamma_w \left[(\sigma - \sigma' V^T x) e_x^T + \lambda_w \|e_x\| W \right] \\ \dot{V} &= -\gamma_v \left[x e_x^T W^T \sigma + \lambda_v \|e_x\| V \right] \end{aligned} \quad (16)$$

where e_x are state errors and $\gamma_w, \gamma_v, \lambda_w, \lambda_v$ are design parameters (learning rates and e-modification factors).

2.5. The Sigma Pi Neural Network

The third and final neural algorithm investigated in this effort is a two-layer Sigma-Pi NN^{9,10,11} for each angular acceleration ($\dot{p}, \dot{q}, \dot{r}$). These NNs feature proportional and integral acceleration errors ($U_{p_error}, U_{q_error}, U_{r_error}$) for on-line learning purpose:

$$U_{x_error} = \left(K_{p_{x_error}} + \frac{K_{i_{x_error}}}{s} \right) \cdot e_x \quad x = p, q, \text{ or } r \quad (17)$$

Inputs to the networks are pseudo control acceleration commands (U_p, U_q, U_r), bias terms, and sensor feedback. For each channel three terms C_1, C_2 and C_3 are computed as functions of input variables and previous-step network outputs ($U_{pad}, U_{qad}, U_{rad}$):

$$C_{1_x} = bias, V_t, V_t^2, h \quad (18)$$

$$C_{2_p} = bias, \frac{1 - e^{-(U_p - U'_{pad})}}{1 + e^{-(U_p - U'_{pad})}}, p, r, p_{ref} \quad (19)$$

$$C_{2_q} = bias, \frac{1 - e^{-(U_q - U'_{qad})}}{1 + e^{-(U_q - U'_{qad})}}, q, q_{ref} \quad (20)$$

$$C_{2_r} = bias, \frac{1 - e^{-(U_r - U'_{rad})}}{1 + e^{-(U_r - U'_{rad})}}, p, r, r_{ref} \quad (21)$$

$$C_{3_x} = bias, \alpha, \beta \quad x = p, q, r \quad (22)$$

All the neuron outputs are summed and multiplied to each other – from which the name of the NN topology originates. The outputs of the NNs are the control augmentation commands defined as:

$$U_{ad} = W^T f(C_1, C_2, C_3) \quad (23)$$

where f is computed from each signal inputs using a nested Kronecker product. The network weights W are determined by an adaptation law:

$$\dot{W} = -G(U_{error} \cdot f + L|U_{error}|W) \quad (24)$$

where G and L are user selected specific gains.

2.6. Results of the Comparative Study

An extensive simulation study has been performed using the WVU IFCS F-15 ‘Gen_2’ flight simulator³. Only a subset of the simulation results are here presented for brevity purposes for illustrating the main conclusions.

The simulations have been performed at Mach = 0.75 and altitude = 20000 ft., which is to be considered the single-point flight condition at which most of the research flight test maneuvers will be performed. Following interaction with the technical monitor, 6 specific test cases have been considered:

Case #1: nominal conditions, no failure, doublets on all three channels;

Case #2: right stabilator locked at -4 degree at $t=40$ s, no pilot input;

Case #3: right stabilator locked at -4 degree at $t=40$ s, doublets on all three channels, before and after the failure;

Case #4: right stabilator locked at +8 degree at $t=40$ s, no pilot input;

Case #5: left canard locked at -4 degree at $t=40$ s, no pilot input;

Case #6: left canard locked at -4 degree at $t=40$ s, doublets on all three channels, before and after the failure.

The mean values and the standard deviations of the errors between reference model angular rates and actual aircraft angular rates have been computed for assessing the performance of the different approaches. The results for the roll, pitch, and yaw channels are presented in Tables 1-3, respectively.

The NLDI-based controller is coping with the failure in all the cases investigated except Case #4. A similar behavior is recorded for the Sigma Pi augmented version. The EMRAN and SHL augmented versions can handle all the cases investigated.

On the roll and pitch channel the best performance are achieved using the EMRAN NN with the SHL-augmented and the SP-augmented control laws ranking second and third respectively.

On the yaw channel the SHL-augmented control laws outperform the others.

As an example, Figure 1 shows the time histories of the square of the pitch rate tracking errors for the three NNs and with the NN off for the stabilator failure case (case #2). A similar plot is presented in Figure 2 for the canard failure case (case #5). The time histories of the square of the roll rate tracking errors for the same two cases are shown in Figure 3 and 4 respectively.

2.7. Conclusions

The performance associated with the augmentation of 3 different NNs for the 'Gen_2' DI-based control laws have been compared. The neural augmentation is designed to assist the DI control laws at post failure conditions.

Different failure scenarios for the IFCS F15 stabilators and canards have been investigated. Each of the considered neural algorithms has shown to provide successful augmentation of the DI-based control laws leading to better dynamic responses at post failure conditions – compared with the NN off case.

The results shown that the EMRAN algorithm slightly outperforms the other two algorithms in terms of the angular rate tracking errors, while requiring a lower computational effort.

3. Safety monitor schemes for transition to research control laws

3.1 Introduction

The IFCS F-15 'Gen_2' control laws are based on the use of NNs to augment a NLDI based controller^{1,16,17}. The role of the NNs is to compensate for inversion errors and changes in aircraft dynamics due to the injection of the failure on a primary control surface. In this document this set of control laws will be referred to as the "research control laws" (RCL), while the basic (background) control laws will be denoted as the "conventional control laws" (CCL). The RCL are implemented on a dedicated "research flight computer" (RFC) – the ARTS2 on-board computer - while the CCL are installed on the "basic flight computer" (BFC) – the SC3 on-board computer.

The flight testing of the RCL implies the switching by the pilot at a certain instant from the CCL to the RCL at nominal conditions and – at a later instant - the switching from the RCL at nominal conditions to the RCL with simulated failures on specific control surfaces. The risks associated with these transitions and the need for a logic to decide whether the transitions can be safely performed have been acknowledged within the flight control testing community¹⁸⁻²⁰.

In recent years, flight control systems for different test aircraft have been provided with a scheme to monitor the safety of the transitions described above (e.g. F-16 Variable Stability In-Flight Simulator Test Aircraft - VISTA and F/A-18 High Angle of Attack Research Vehicle - HARV).

The specific characteristics related to the operation under simulated control surface failure have led to the development of two different sub-schemes (SM#1 and SM#2). Their logic, for the different transitions, uses information relative to different parameters, such as flight conditions and controller-related performance criteria.

3.2. Description of the "Safety Monitor" Scheme

At any point in the flight envelope the aircraft control laws are assumed to be in one of the following modes:

- *Nominal Mode* (NM)
- *Research Mode* (RM)
- *Simulated Control Surface Failure Mode* (FM).

The existence of these distinct modes of operation implies the need for a total of five different switch logics: NM to RM and back, RM to FM and back, and FM to NM. Note that the direct transition from NM to FM is not allowed. The issues and the risks related to these transitions are different; therefore, two separate safety monitor schemes have been developed (SM#1 and SM#2). In particular, the SM#1 scheme handles the transition from NM to RM while SM#2 handles the remaining transitions.

3.2.1. Operation Modes

The characteristics of the three operating modes of the IFCS F-15 aircraft during the test flight are as follows:

- **Nominal Mode** (NM): the conventional control laws (CCL) implemented in the basic flight computer (BFC) are active and the SM#1 decides whether transition to Research Mode (RM) is safe. The test flight is initiated in the NM.

- **Research Mode** (RM): the research control laws (RCL) implemented in the research flight computer (RFC) are active and the SM#2 decides whether the transition to Simulated Failure

Mode (FM) is safe – OR – the RM should be maintained – OR – the RM should be aborted with re-engagement of the NM mode.

- ***Simulated Control Surface Failure Mode (FM)***: the RCL implemented in the RFC are active and a failure of a primary control surface is simulated. The control surface subjected to the simulated failure is selected by the pilot. The SM#2 decides whether maintaining the FM is safe – OR - the simulated failure should be disengaged - AND - either the RM or the NM should be re-engaged. The re-engagement of the RM or the NM is performed automatically by the SM.

3.2.2. Abnormal Situations

The decisions by the two SMs are based on the analysis of a large set of dynamic parameters selected to provide detectability of abnormal situations which do not allow the safe operation of the RFC and the RCL under nominal and/or failure conditions. Such abnormal situations include failures of various aircraft sub-systems (other than the control surfaces), suspect functioning of different sub-systems, and operations at unsafe flight conditions.

The abnormal situations have been grouped in nine categories. In general, a "red" or a "green" flag is associated to each category depending on whether abnormal situations exists or not.

Category #1 - any failure for the Flight Control System (FCS) (including sensor failures and actuator failures – for other surfaces excluding stabilators and canards), the propulsion system, the electrical system, etc. The SM is provided with failure flags from distinct failure detection and identification (FDI) schemes.

Category #2 - failures reported from the RFC. The failure flag is generated and sent to the SM by a failure detection scheme associated with the RFC.

Category #3 – exceedance of a pre-assigned flight envelope within which the flight testing should be restricted. The allowed flight envelope is defined in terms of Mach number and altitude.

Category #4 - aircraft dynamic characteristics exceeding certain pre-imposed limits. The dynamic characteristics considered are: linear accelerations, angular rates, angle of attack, and sideslip angle.

Category #5 – inappropriate aircraft configurations for safe flight testing, such as center of gravity exceeding certain ranges, low levels of fuel, landing gear up, flaps up, speed brakes up, etc.

Category #6 - failures of the data communication bus.

Category #7 - inaccurate tracking of commanded angular rates due to poor performance of the BCL. Since in this study both CCL and RCL feature command augmentation systems, it is appropriate to use tracking information for assessing normal/abnormal operations. In particular, both the tracking errors and their rates are expected to remain within certain limits on all three channels (roll, pitch, and yaw). The bounds are variable and are computed based on statistics of the signals using a "Floating Limiter" (FL) concept outlined in the next section.

Category #8 – excessive control activity for primary control surfaces (without the injection of the failure). Individual control surfaces are considered (left and right stabilator, canard, aileron, and rudder). A floating limiter augmented with a saturation proximity limiter is used. Additionally, or as an alternative, the pseudo-control hedging^{21,22} (PCH) activity can be used as an index of normal/abnormal operation of the control surfaces.

Category #9 - excessive levels of activity for the NNs augmenting the NLDI controllers. The activity of the NN is evaluated in terms of the sum of the NN weights, the sum of the

updates of the NN weights, and the NN outputs. For the three channels, this adds up to a total of nine signals that are provided as inputs to floating limiters, respectively.

It should be emphasized that categories #1 to #6 can be associated only with "green" or "red" flags. For categories #7 to #9 the floating limiter can be used to generate cautionary and failure bounds. If 'cautionary bounds' – later defined - are exceeded, then a "yellow" flag is declared. If 'failure bounds' – also later defined - are exceeded, then a "red" flag is declared instead. The particular actions taken by the SM as a consequence of these different flags are described in §3.2.4 and §3.2.5.

It is assumed that the abnormal situations relative to categories #1, #2, #5, and #6 are detected by other FDI schemes, while the rest of the categories are assessed using the SM presented in this paper.

3.2.3. Floating Limiter

The logic of the SM scheme is based on the use of the "Floating Limiter" (FL) concept. The FL uses statistical parameters of a signal to compute upper and lower bounds of the acceptable domain of operation. This domain has two levels of boundaries, that is cautionary and failure bounds. When these bounds are exceeded, the SM takes the actions described in the next section. The signal to be monitored along with its derivative are filtered to obtain approximations of their average values and standard deviations. Then, the cautionary upper and lower bounds (CUB and CLB, respectively) along with the failure upper and lower bounds (FUB and FLB, respectively) are computed using the relationships:

$$\begin{aligned} \text{CUB}(x) &= \bar{x} + b_c \cdot \sigma(x) + \text{bias} \\ \text{CLB}(x) &= \bar{x} - b_c \cdot \sigma(x) - \text{bias} \\ \text{FUB}(x) &= \bar{x} + b_f \cdot \sigma(x) + \text{bias} \\ \text{FLB}(x) &= \bar{x} - b_f \cdot \sigma(x) - \text{bias} \end{aligned} \tag{25}$$

where \bar{x} is the average value of x , $\sigma(x)$ is the standard deviation of x , b_c is the cautionary bound factor, b_f is the failure bound factor. Similar relationships are used for the derivative of x .

In order to declare a failure or a cautionary situation, the respective bounds must be exceeded for a number of times n over a time window of width t_n . This will prevent false alarms following accidental bound exceedence due to perturbations and/or noise.

When a simulated control surface failure is engaged, the parameters involved in the categories #7, #8, and #9 exhibit relatively large transients. This will usually determine the exceedence of the bounds and the disengagement of the simulated failure. To avoid such a situation the bounds computed in (25) are relaxed for a duration t_{rel} following the moment the failure is engaged. This is achieved by allowing larger values for the bound factors (b_c, b_f) and the bias.

The block diagram of the floating limiter is presented in Figure 5. The Simulink scheme of the floating limiter is shown in Figure 6. It is used as a building block for the SM components assessing abnormal situations in the categories #7, #8, and #9.

3.2.4. Subscheme #1 (SM#1)

The SM #1 has the objective of supervising the transition from the CCL and the BFC to the RCL at nominal conditions and the RFC, in other words the transition from NM to RM. SM#1 operates only while the aircraft is in NM and monitors the occurrence of abnormal situations in the categories #1 to #7. If all the flags are "green" then the transition from NM to RM is allowed and can be performed if the pilot wishes to do so. If any of the flags is "red" or the category #7 flag is "yellow" then the transition from NM to RM is not allowed and the flight must continue in NM. Figure 7 shows the block diagram relative to the SM#1.

3.2.5. Subscheme #2 (SM#2)

The SM#2 has the task of supervising all the other four possible transitions except the transition from NM to RM. SM#2 operates while the control laws are in RM and FM. It monitors the occurrence of abnormal situations in the categories #1 to #9.

Consider the test aircraft in RM. If all the flags are "green" then the transition from RM to FM is allowed and a simulated primary control surface failure can be engaged at any time by the pilot. The pilot can also select to switch back to NM. If any of the flags is "red" then the SM#2 will automatically switch back to NM, disengage the RCL/RFC, and reengage CCL/BFC. If any of the flags of categories #7 to #9 is "yellow" the transition from RM to FM is not allowed; however RM is allowed to continue.

If the test aircraft is in FM and all the flags are "green" then it is safe to continue to FM. The pilot can of course switch back to RM or NM at any time. If any of the flags is "red" then the SM#2 will automatically switch back to NM. If any of the flags of categories #7 to #9 is "yellow" then the SM#2 will disengage the simulated failure and switch back to RM.

Figures 8 and 9 illustrate the operation of the SM#2 while the control laws are in RM and FM, respectively.

3.3. Description of the IFCS F-15 Simulation Code

The Matlab/Simulink based WVU IFCS F-15 Simulation Code features a non-linear model of the NASA F15 dynamics featuring a set of look-up tables describing the aerodynamic characteristics of the aircraft. Failures of the primary control surfaces are modeled using an approach based on a modification of their aerodynamic efficiency at post-failure conditions^{23,24}. Each of the eight individual control surfaces can be 'artificially' failed with the following options:

- surface lockage (stuck actuator)
- partial/total destruction of the surface along surface lockage (stuck actuator).

The conventional control laws are generated using a non-linear dynamic inversion (NLDI) based approach. The research control laws are obtained using an adaptive neural controller canceling the errors associated with the dynamic inversion of the aircraft model. Desired characteristics in terms of second order responses for the pitch and directional channels and first order response for the roll channel are achieved with "ad hoc" reference models. A PCH scheme is added to reduce the effects of control saturation. As described in the previous section 3 different types of NNs are implemented (SigmaPi, EMRAN and Single Hidden Layer NN) and can be selected by the user. The values of aerodynamic stability and control derivatives required by the dynamic inversion algorithm can be either kept constant throughout the simulation, corresponding to the initial equilibrium flight condition, or can be updated using a pre-trained NN as the aircraft moves in the flight envelope. This control strategy has been selected to

provide consistent handling qualities without requiring the level of computational effort associated with gain-scheduling or system identification.

Figure 10 shows the main Simulink scheme of the WVU IFCS F-15 'Gen_2' Simulation Code.

3.4. Description of the Interface Between the SM Scheme and the WVU IFCS F-15 Simulator

The user can set the desired simulation scenario through interactive menus. Either nominal flight conditions or failure conditions can be selected. The nominal flight scenario includes only NM and RM thus allowing switching to and from RCL/RFC and CCL/BFC. These actions can be performed by the simulation pilot using the main SM switch (shown in Figure 11). During nominal flight only abnormal situation in the categories #3, #4, and #7 can occur. The "flight with failures" scenario allows operation in the Simulated Control Surface Failure Mode (FM). When FM is engaged by the pilot from the main SM switch, a failure of previously imposed magnitude on the previously selected control surface occurs. Switching back to RM or NM as a result of pilot or SM action will disengage the failure. Unlike this "simulated" failure, a permanent, "real" failure of one of the control surfaces can also be implemented. Its magnitude and time of occurrence is selected by the user before the simulation. When it occurs and is properly detected, the SM declares an abnormal situation of category #1 and takes appropriate action (see Section 3.2). The occurrence of other "real" abnormal situations in the categories #1, #2, #5, and #6 can be imposed at specified times using the failure menu shown in Figure 12. The flags of the abnormal situations are shown during the simulation using the color code (red, yellow, green) as described previously (see Figure 13 for SM#1 and Figure 14 for SM#2).

The parameters of the floating limiter can also be set by the user. Figure 15 shows the corresponding menu with the values used for this study.

The time histories of all the different parameters and flags related to the categories #7, #8, and #9 (tracking errors, control deflections, sum of NN weights and their update rate, NN output) can also be displayed during or after the simulation. The scopes to be displayed can be selected through the menu shown in Figure 16.

3.5. Simulation Results for Different Scenarios

To illustrate the operation of the SM scheme, the results for two different scenarios have been included.

Scenario #1. The first simulation case consists of a series of smooth maneuvers (doublets on the three channels) during the three operation modes without exceeding the bounds of any abnormal situation. During the first 20 seconds, the aircraft is in NM; for the next approx. 20 seconds the aircraft is in RM. At this time, a simulated failure on the right stabilator is engaged (locked stab at -4 degrees). The aircraft remains in FM until approximately $t=65$ s while doublets on all three channels are performed. Next the pilot switches back to RM and the failure is disengaged. After 10 seconds the failure is re-engaged for an other 10 seconds after which the pilot returns to NM. Figures 17 and 18 show the variation of the left and right stabilators, respectively, within the variable cautionary and failure bounds. Note the presence of the failure on the right stabilator. The acceptable bounds are not exceeded except for short periods of time, which does not trigger the declaration of an abnormal situation. Throughout the entire simulation the SM performs as expected.

Scenario #2. The second simulation case includes more demanding pilot inputs that would trigger exceedence of abnormal situations bounds and thus limiting actions from the SM scheme. At 15 s, 30 s, and 50 s the RM is engaged but, after a transient, the acceptable limits of the control activity parameters (category #8) are exceeded; thus, SM#1 switches back to NM. At t=60 s the aircraft is in RM again and at t=70 a simulated failure of the right stabilator (locked at -4 degree) is engaged. At t=75 s the cautionary bounds of category #8 are exceeded and the failure is disengaged while the RM is still maintained. Shortly after, the failure bounds are exceeded as well and a switch back to NM is commanded by the SM#2. Figures 19 and 20 show the deflections of the left and right stabilators, respectively, within the variable cautionary and failure bounds. SM#2 detects that the exceedence of the acceptable bounds has occurred (see Figure 23 for the variation of category #8 flag). Figures 21 and 22 show a typical category #8 abnormal situation due to excessive canard activity.

Even in this case, the SM scheme performed as expected in all situations.

3.6. Simplified SM scheme

During the design, a large number of parameters have been investigated as candidates for safety monitor purposes. Following interaction with the technical monitor, the need to reduce the complexity of the scheme and to simplify the validation task led to a reduction of the signals monitored. Eventually only the angular tracking error of the angular rates (3 signals) and the NN output (3 signals) have been considered. The monitoring of these parameters is based on the concept of floating limiter augmented with a range check and persistence counters.

3.6.1. Simplified floating limiter

The FL has some unique features which allow full authority and rates within a window, but rate limits if the input signal persists in one direction for preventing a hardover from coming through to the control system. The logic of the SM scheme is based on the use of the FL concept as shown in Figure 24. The FL works by computing the rate of change of the input signal to be tested. Upper and lower bounds are placed on the input signal and a drift rate is applied to the FL. The FL will try to center about the input signal and drift with it at a rate equal to the rate of the signal but less than an imposed limit. High rate of changes are permitted only within floating limiter upper and lower bounds.

The upper bound (UB) at time step 'n' is:

$$UB(n) = \min \left(\begin{array}{l} s(n) + \Delta(s) \\ UB(n-1) + R_{\max}(s) \times [t(n) - t(n-1)] \end{array} \right) \quad (26)$$

The lower bound (LB) at time step 'n' is:

$$LB(n) = \max \left(\begin{array}{l} s(n) - \Delta(s) \\ LB(n-1) - R_{\max}(s) \times [t(n) - t(n-1)] \end{array} \right) \quad (27)$$

where ' Δ ' represents the range within which the signal is allowed to vary at any rate, and R_{\max} represents the maximum rate at which the bounds are allowed to vary. Both these parameters depend on the nature of the input signal but are constant in time. Figure 25 shows an example of the input signal changing in the positive direction at the maximum rate of the FL; therefore, it can keep up with the signal and remain centered. The signal then changes in the negative direction at a rate greater than the FL. The drift rate of the FL cannot keep up and the signal approaches the FL lower bound. Before it reaches the FL lower bound, it changes at a high rate in the positive direction. The FL reverses direction, again. Finally, the input signal reaches the upper bound of the FL and is 'clamped' to this value. A persistence counter starts at the moment the bound is reached. For this example, the persistence counter limit is 3 and a red flag (down mode from RCL to CCL) is set. If the input signal had reversed before the persistence counter limit was reached, the counter would have reset back to zero.

3.6.2. Range Limiter

A range monitor is used to check signals that change at a slow rate, which the FL would not detect. In other words, if the monitored signal varies at a low rate it could grow indefinitely. To avoid such situation, the FL is augmented with a range check. This will limit the values of the FL bounds at imposed constant values.

3.6.3. Persistence Counter

As soon as a bound is reached, the monitored signal is limited. However, in order to avoid a large number of nuisance disengagements, the operation is allowed to continue as before. Down mode is not triggered unless the bounds are exceeded for a selected time interval (in Figure 25 this interval is '3' sampling steps). The persistence counter totals the number of consecutive hits, then a flag is sent to down mode to CCL when the limit is reached.

3.6.4 Reduced number of parameters monitored

Two categories of parameters have been investigated for safety monitor purposes in this study. The first are parameters related to the tracking error (TE) of the angular rates. The second are the parameters related to the operation of the NNs.

The tracking error parameters were the statistics of the TE (mean and standard deviation) and the TE itself. Initially, both these signals and their variation rate were considered. For the three channels (roll, pitch, and yaw) this adds up to a total of 18 different signals.

The NN parameters considered initially were the NN output, the sum of the NN weights, and the sum of the NN weight update rates. These parameters and their rates add up to a total of 18 monitored signals.

The variation of the FL metrics for these monitored signals have been determined with the goal to achieve maximum "correct detection"/"false alarm" ratios. Through extensive simulation it has been determined that none of these parameters is redundant. Any of the monitored parameters can be the first to detect an abnormal situation. To illustrate this point, two control surface failure cases are shown in Figures 26-29. In case #1 the NN output based criterion detects the abnormal situation while the sum of the NN weights fails. In case #2 however, the situation reverses.

The need to reduce the complexity of the scheme and to simplify the validation task has lead to a reduction of the signals monitored. Only the angular tracking error of the angular rates (3 signals) and the NN output (3 signals) have been considered. Abnormal situations will be

reflected in this set of parameters. Monitoring more signals can reduce the time of detection, but this effect can also be achieved by appropriate tuning of the FL parameters at the expense of increased false alarm rate.

3.6.5. Testing of the simplified scheme

To illustrate the operation of the SM scheme a 20 sec simulation has been performed which included input doublets of moderate amplitude on all three channels. At time=7 sec the right stabilator is locked at the current trim position plus 4 degrees. At time=15 sec the simulated failure is disengaged. Note that all the parameters of the SM used here were tuned only for test purposes and to provide an example of the operation of the SM.

The time histories of the safety monitor flags on the roll channel are presented in Figure 30. The range check flag of the roll rate tracking error turns '*red*' (=is set to 1) at time=9.1625, that is 0.125 sec after the range limit is exceeded (see Figure 31). It becomes '*red*' again at time=15.15 due to the exceedence of the FL limits (see Figure 31). Figure 32 shows the operation of the FL on the NN output on the roll channel. The FL upper bound is exceeded at $t=15.275$ and the corresponding flag turns '*red*' at $t=15.4$. The 'clamping' of the signals occurs as expected for both the tracking error (Figure 33) and the NN output (Figure 34). Note that the 'clamping' of the signal is not subject to the persistence condition and it is performed as soon as the limits are exceeded.

3.7. Conclusions

A general Safety Monitor (SM) scheme has been designed to ensure safety while evaluating experimental control laws. A comprehensive set of abnormal situations has been assessed based on external and internal detection schemes. The resulting safety monitor scheme uses a floating limiter with double level limits to determine acceptable variable bounds for significant parameters, based on past time histories and statistics. Throughout extensive simulations, the approach has shown to be efficient and reliable.

The simulations of two different flight scenarios have been performed using the WVU IFCS F-15 Simulink based simulator. In both cases, the SM scheme has provided very desirable performance.

A simplified monitor scheme has been designed with only 6 parameters and a single level floating limiter. Issues related to the reduction of the scheme complexity have been analyzed extensively with the technical monitor.

The design concept of the FL allows tuning for the particular input signals. The upper and lower boundaries, drift rate, and persistence counter limit can be adjusted in real time as necessary according to the simulated failure dynamics.

The operation of the scheme has been tested through simulation and the approach has shown to be efficient, reliable, and easily tailored to specific applications including simulated failures in a piloted simulation environment.

4. Modifications to Remove Cross-Coupling Issues on the IFCS F-15 Control Laws

4.1. Introduction

In late Fall 2003 reports from the pilot in the NASA simulator indicated that a persistent cross coupling induced by stabilator failure was present at post-failure conditions. The solution proposed by WVU researchers for reducing the dynamic coupling was based on the introduction of coupling terms (CCT) in the cost function of the neural networks. Therefore, products of the angular rates and angular rate cross correlations have been considered as possible coupling terms to be added to the cost function.

4.2. Cross-coupling parameters

Non-zero products of the angular rates naturally reflect the occurrence of a dynamic coupling. The use of the coefficients of the cross correlation function has also been investigated for the same purpose. This may still be a path worth searching although preliminary results did not show too much difference. However, the cross correlation is used to assess the “amount” of coupling and the performance of the scheme.

If the tracking would be perfect, there would be no coupling. Therefore, the tracking error part of the cost function should have a large numerical weight, and the coupling term should enhance its effect. Thus, cross-coupling terms are added to the tracking error to form the cost function of the NN. For the roll, pitch, and yaw channels respectively the cross-coupling term is expressed as:

$$\begin{aligned} k_{\text{roll}} \cdot |p \cdot q| \cdot \text{sign}(p_{\text{err}}) \\ k_{\text{pitch}} \cdot |p \cdot q| \cdot \text{sign}(q_{\text{err}}) \\ k_{\text{yaw}} \cdot |r \cdot q| \cdot \text{sign}(p_{\text{err}}) \end{aligned} \quad (28)$$

where ‘p’, ‘q’, and ‘r’ are the angular rates, the k’s are proportional gains, and p_{err} and q_{err} are roll and pitch rate tracking errors. It has been noticed that occasionally the coupling terms would tend to “fight” the tracking error since they might have different sign; therefore, an adaptive sign for the coupling term has been introduced by multiplying the absolute value of the coupling term with the sign function of the tracking error. It should be underlined that a drawback of this approach is the possibility of discontinuities (jumps) in the cost function whenever the tracking error changes sign. No adverse effect has been noticed in the limited amount of simulations performed; however, a smoothing filter could be introduced to handle this problem.

4.3. Simulation results

4.3.1. Test Case #1

Failure: +4 deg right stab at $t=10$ sec, removed at $t=20$ sec. Augmenting NN: SHL. Mach=0.75.

Pilot input: doublets on pitch channel only

Table 4 presents the statistics (mean and standard deviation) of the tracking error as a measure of the performance of the scheme in 3 distinct situations:

- NN off
- SHL-NN on without cross-coupling terms (CCT)
- SHL-NN on with cross-coupling terms (CCT).

It should be noted that there are no significant reduction in the mean; however, this parameter was small from the beginning. On the other side there is significant reduction in the standard deviation for SHL-NN on with the CCT as compared to the “NN off” case and the “SHL-NN on without CCT” case. These results are illustrated in Figures 35-37.

Table 5 presents the effects of adding CCT terms on the cross-correlation. Slight performance deteriorations can be observed in terms of pitch/yaw dynamic coupling. However, this coupling was negligible to start with. On the other side, a significant reduction is obtained for the roll/pitch coupling. These results are illustrated in Figures 38-40.

4.3.2. Test Case #2

Failure: +4 deg right stab at $t=10$ sec, removed at $t=50$ sec

Augmenting NN: SHL. Mach=0.75. Pilot input: doublets on pitch channel only.

Improvements in the statistics of the tracking error (see Table 6) and in the cross-correlation parameter (see Table 7) are observed. These improvements are better than those achieved for Case #1. However, the absolute values of the parameters monitored are reduced. Figures 41 to 43 show the time histories of the square of the angular rate tracking errors. Figures 44 to 46 show the time histories of the angular rate cross correlations.

4.3.3. Test Case #3

Failure: right stab locked at trim, at $t=10$ sec

Augmenting NN: SHL. Mach=0.75. Pilot input: doublets on pitch channel only

The statistics of the tracking errors are presented in Table 8. The effect of the CCT in term of percentual variation of the angular rate cross correlation is presented in Table 9. There is no improvement but the considered parameters (tracking error and CC parameter) have very low values as compared to the two previous cases.

4.4 Conclusions

Cross-coupling terms have been defined in terms of weighted cross products of the angular rates to be added to the cost function of the NN to improve the cross axes response. An adaptive sign was introduced to avoid counteracting actions by the tracking error and the CCT. The addition of the adaptive sign actually improve the performance substantially.

Simulations show performance improvement in terms of cross-coupling reduction evaluated by means of angular rate cross-correlation and tracking error.

References

1. Perhinschi M. G., Burken J., Napolitano M.R., Campa G., Fravolini M. L., "Performance Comparison of Different Neural Augmentation for the NASA Gen_2 IFCS F-15 Control Laws", accepted for presentation at the *American Control Conference 2004* Boston MA
2. Perhinschi M. G., Napolitano M.R., Stolarik B., Hammaker S., Campa G., Rogers S., "Design Of Safety Monitor Schemes for a Fault Tolerant Flight Control System", *Proceedings of the AIAA Guidance, Navigation, and Control Conference*, August 2003, Austin, Texas, AIAA-2003-5646
3. Perhinschi M. G., Napolitano M.R., Campa G., Fravolini M. L., "A Simulation Environment for Testing And Research of Neurally Augmented Fault Tolerant Control Laws Based on Non-Linear Dynamic Inversion", accepted for presented at the *AIAA Modeling and Simulation Technologies Conference*, 2004 Providence RI
4. Burken J., Perhinschi M. G., Napolitano M.R., Campa G., Fravolini M. L., Burke, H. E., Larson R. R., "Design and Testing of a Safety Monitor Scheme on the NASA Gen_2 IFCS F-15 Flight Simulator", submitted to the *American Control Conference 2004* Boston MA
5. "Intelligent Flight Control: Advanced Concept Program – Final Report", The Boeing Company, BOEING-STL 99P0040, May 1999.
6. Calise A. J., Lee S., Sharma M., "Direct Adaptive Reconfigurable Control of a Tailless Fighter Aircraft", *Proc. of the 1998 AIAA Guidance, Navigation and Control Conference*, Boston MA, August 1998, AIAA 98-4108
7. Rysdyk R.T., Calise A. J., "Fault Tolerant Flight Control via Adaptive Neural Network Augmentation", AIAA 98-4483, August 1998.
8. Calise A. J., Sharma M., "Adaptive Autopilot Design for Guided Munitions", *AIAA Journal of Guidance, Control and Dynamics*, vol. 23 no 5, 2000
9. Kaneshige J., Bull J., Totah J.J., "Generic Neural Flight Control and Autopilot System", AIAA Paper 00-4281, Denver, Co, August 2000.
10. Kaneshige J., Gundy-Burlet K., "Integrated Neural Flight and Propulsion Control System", AIAA Paper 01-4386
11. Lu Y., Sundararajan N., Saratchandran P., "Analysis of Minimal Radial Basis Function Network Algorithm for Real Time Identification of Nonlinear Dynamic Systems", *IEEE Proceedings on Control Theory and Application 2000*, vol.4, no 147, pp.476.
12. Shin Y., Ghosh J., "The Pi-Sigma Network: An Efficient Higher-Order Neural Network for Pattern Classification and Function Approximation", IEEE 7803-0164, 1991.
13. Campa G., Fravolini M.L., Napolitano M.R., "A Library of Adaptive Neural Networks for Control Purposes", IEEE International Symposium on Computer Aided Control System Design, September 18-20, 2002 Glasgow, Scotland, UK.
14. Fravolini M.L., Campa G., Napolitano M.R., La Cava M., "Comparison of Different Growing Radial Basis Functions Algorithms for Control Systems Applications", *Proc. of the 2002 American Control Conference*, Anchorage AK, May 2002
15. Polycarpou M., "On-Line Approximators for Nonlinear System Identification: A unified Approach", *Control and Dynamic Systems Series*, vol. 7, Ac. Press, Jan. 1998
16. Perhinschi M. G., Campa G., Napolitano M. R., Fravolini M. L., Lando M., Massotti L., "Performance Comparison of Fault Tolerant Control Laws Within the NASA IFCS F-15 WVU Simulator", submitted to the American Control Conference 2003

17. Perhinschi M. G., Napolitano M. R., Campa G., Fravolini M. L., Massotti L., Lando M., "Augmentation of a Non Linear Dynamic Inversion Scheme Within the NASA IFCS F-15 WVU Simulator ", submitted to the American Control Conference 2003
18. Carter J. F., "Production Support Flight Control Computers: Research Capability for F/A-18 Aircraft at Dryden Flight Research Center", NASA-TM-97-206233, Oct. 1997
19. Carter J. F., Stephenson M., "Initial Flight Test of the Production Support Flight Control Computers at Dryden Flight Research Center", NASA-TM-1999-206581, Aug. 1999
20. Minor J., Thurling A. J., Ohmit E., "VISTA - A 21st Century UAV Testbed", United States Air Force Test Pilot School website: <http://www.edwards.af.mil/tps/VISTA/VISTA-21st%20Century%20UAV%20Testbed.pdf>
21. Calise A. J., Sharma M., "Adaptive Autopilot Design for Guided Munitions", *AIAA Journal of Guidance, Control and Dynamics*, vol. 23 no 5, 2000
22. Calise A. J., Lee H, Kim N, "High Bandwidth Adaptive Flight Control", Proc. of the 2000 AIAA Guidance, Navigation and Control Conference AIAA 2000-4551, Denver CO, August 2000
23. Perhinschi M. G., Campa G., Napolitano M.R., Lando M., Massotti L., Fravolini M. L., "Modeling and Simulation of Failures for Primary Control Surfaces", AIAA2002-4786 AIAA *Proceedings of the AIAA Modeling and Simulation Conference*, Monterey, CA 2002
24. Perhinschi M. G., Campa G., Napolitano M.R., Lando M., Massotti L., Fravolini M. L., "Modeling and Simulation of a Fult Tolerant Flight Control System", accepted for publication in the *International Journal of Modelling and Simulation*, Jun. 2004

	NN off		EMRAN		SigmaPi		SHL	
	Mean [deg/s]	STD	Mean [deg/s]	STD	Mean [deg/s]	STD	Mean [deg/s]	STD
Case #1	0.0182	4.4121	-0.0006	3.4229	-0.0086	6.2877	-0.0003	4.0883
Case #2	-0.1369	1.3007	-0.0002	0.8416	-0.0411	1.6936	-0.0003	0.9167
Case #3	-0.0974	4.9750	-0.0028	4.0092	-0.0086	6.2877	-0.0000	5.3922
Case #4	unstable	unstable	-0.0004	1.3014	unstable	unstable	-0.0024	1.5490
Case #5	0.0133	0.1694	-0.0001	0.1640	0.0087	0.1893	-0.0001	0.1549
Case #6	0.0303	4.2208	0.00002	3.4009	0.0054	3.7050	-0.0002	3.0629

Table 1. Performance Parameters on the Roll Channel for the Three NNs

	NN off		EMRAN		SigmaPi		SHL	
	Mean [deg/s]	STD	Mean [deg/s]	STD	Mean [deg/s]	STD	Mean [deg/s]	STD
Case #1	0.0399	0.5059	0.0055	0.5948	0.0100	0.9903	-0.00002	0.6785
Case #2	-0.0651	0.8689	-0.00001	0.4959	-0.0180	0.7122	-0.00003	0.5031
Case #3	-0.0446	1.0112	-0.0334	0.8536	0.0100	0.9903	0.0000	0.9599
Case #4	unstable	unstable	0.9113	0.8593	unstable	unstable	0.5288	0.8285
Case #5	0.0502	0.2589	-0.0000	0.1813	0.0075	0.2806	-0.0000	0.1900
Case #6	0.0037	0.6640	0.0005	0.4781	0.0001	0.6267	-0.0001	0.5094

Table 2. Performance Parameters on the Pitch Channel for the Three NNs

	NN off		EMRAN		SigmaPi		SHL	
	Mean [deg/s]	STD	Mean [deg/s]	STD	Mean [deg/s]	STD	Mean [deg/s]	STD
Case #1	-0.0040	1.6987	0.0077	2.5394	-0.0033	1.7476	-0.0000	0.8324
Case #2	-0.0178	0.2168	-0.0000	0.1577	-0.0088	0.2506	-0.0001	0.1676
Case #3	-0.0093	1.6516	0.0023	2.5565	-0.0033	1.7476	-0.0001	1.0185
Case #4	unstable	unstable	-0.00003	0.2715	unstable	unstable	0.00006	0.3673
Case #5	-0.0156	0.1559	-0.0001	0.1531	-0.0097	0.1603	-0.0001	0.1518
Case #6	-0.0192	1.7560	0.0049	2.5586	-0.0112	1.8180	-0.0001	1.0121

Table 3. Performance Parameters on the Yaw Channel for the Three NNs

		NN off	SHL+CCT	SHL
Roll Channel	Mean	0.0154	-0.1030	0.0107
	STD	7.6556	4.8250	5.6282
Pitch Channel	Mean	0.0004	-0.0017	-0.0014
	STD	1.2662	1.0204	1.0339
Yaw Channel	Mean	-0.5032	-0.3335	-0.2017
	STD	1.1037	0.6142	0.7103

Table 4. Effect of Cross-Coupling Terms Addition - Tracking Error Statistics - Test Case #1

	NN off	SHL	SHL+CCT
Roll/Pitch	100%	79%	62%
Pitch/Yaw	100%	97%	117%
Roll/Yaw	100%	78%	64%

Table 5. Effect of Cross-Coupling Terms Addition - Maximum Cross-Correlation - Test Case #1

		NN off	SHL+CCT	SHL
Roll Channel	Mean	0.0653	0.0597	0.0522
	STD	8.6856	6.1325	6.8776
Pitch Channel	Mean	0.0004	0.0148	0.0007
	STD	1.5091	1.1935	1.2168
Yaw Channel	Mean	-2.1851	-0.4973	-0.8416
	STD	1.5951	0.8350	0.9312

Table 6. Effect of Cross-Coupling Terms Addition - Tracking Error Statistics - Test Case #2

	NN off	SHL	SHL+CCT
Roll/Pitch	100%	77%	58%
Pitch/Yaw	100%	64%	44%
Roll/Yaw	100%	78%	64%

Table 7. Effect of Cross-Coupling Terms Addition - Maximum Cross-Correlation - Test Case #2

		NN off	SHL+CCT	SHL
Roll Channel	Mean	-0.0026	0.0041	-0.0017
	STD	2.2326	2.4536	2.3890
Pitch Channel	Mean	0.0011	0.0106	-0.0002
	STD	0.8308	0.7521	0.7374
Yaw Channel	Mean	-0.0120	0.0015	-0.0014
	STD	0.1288	0.1762	0.1580

Table 8. Effect of Cross-Coupling Terms Addition - Tracking Error Statistics Test Case #3

	NN off	SHL	SHL+CCT
Roll/Pitch	100%	109%	116%
Pitch/Yaw	100%	127%	133%
Roll/Yaw	100%	125%	144%

Table 9. Effect of Cross-Coupling Terms Addition - Maximum Cross-Correlation - Test Case #3

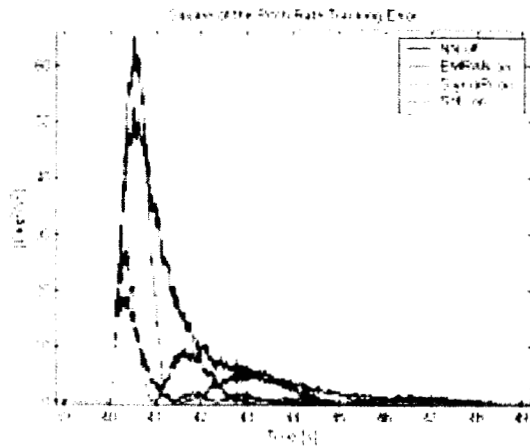


Figure 1. Comparison of the three NNs - Stabilator failure at $t=40s$ - Pitch Channel

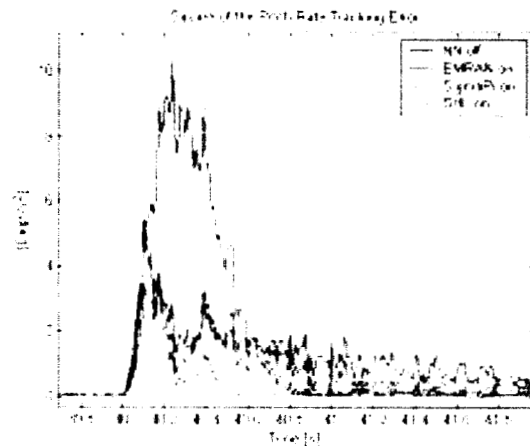


Figure 2. Comparison of the three NNs - Canard failure at $t=40s$ - Pitch Channel

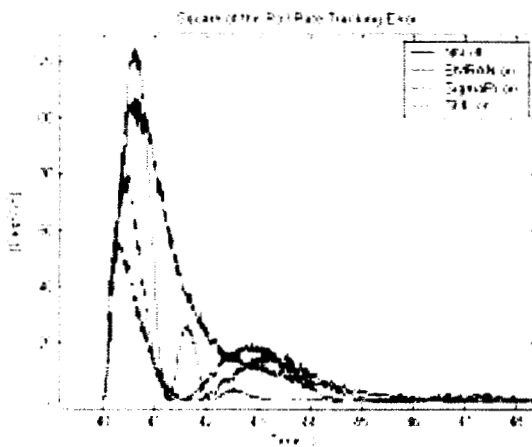


Figure 3. Comparison of the three NNs - Stabilator failure at $t=40s$ - Roll Channel

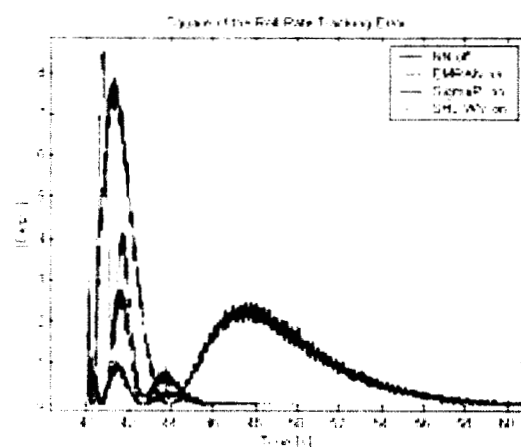


Figure 4. Comparison of the three NNs - Canard failure at $t=40s$ - Roll Channel

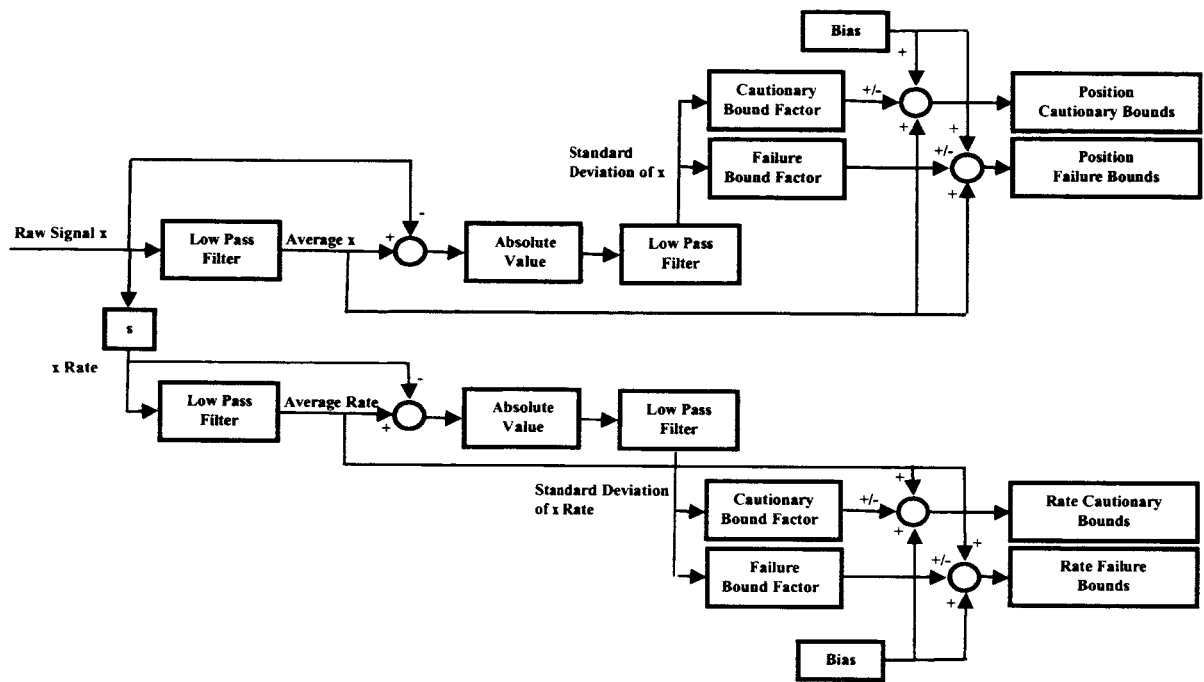


Figure 5. Block diagram of the Floating Limiter

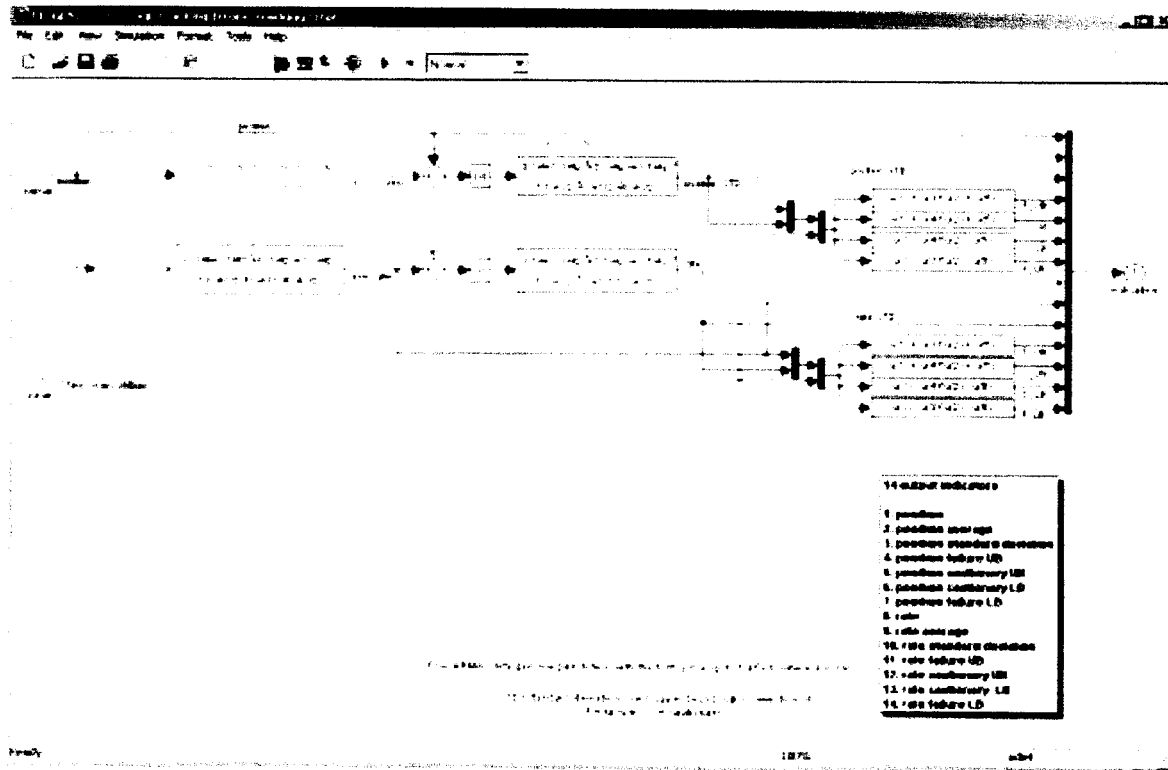


Figure 6. Simulink Implementation of the Floating Limiter

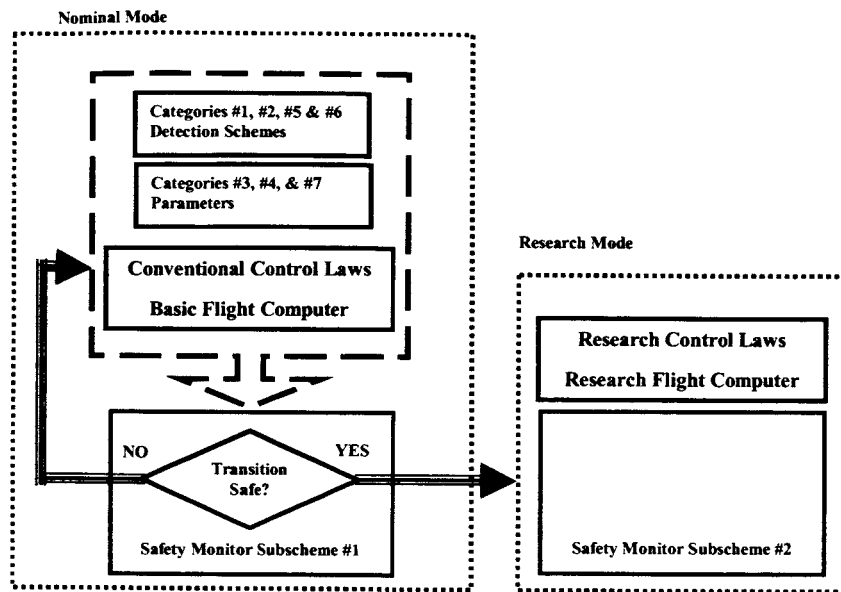


Figure 7. Block Diagram of the Safety Monitor Scheme #1 (SM#1)

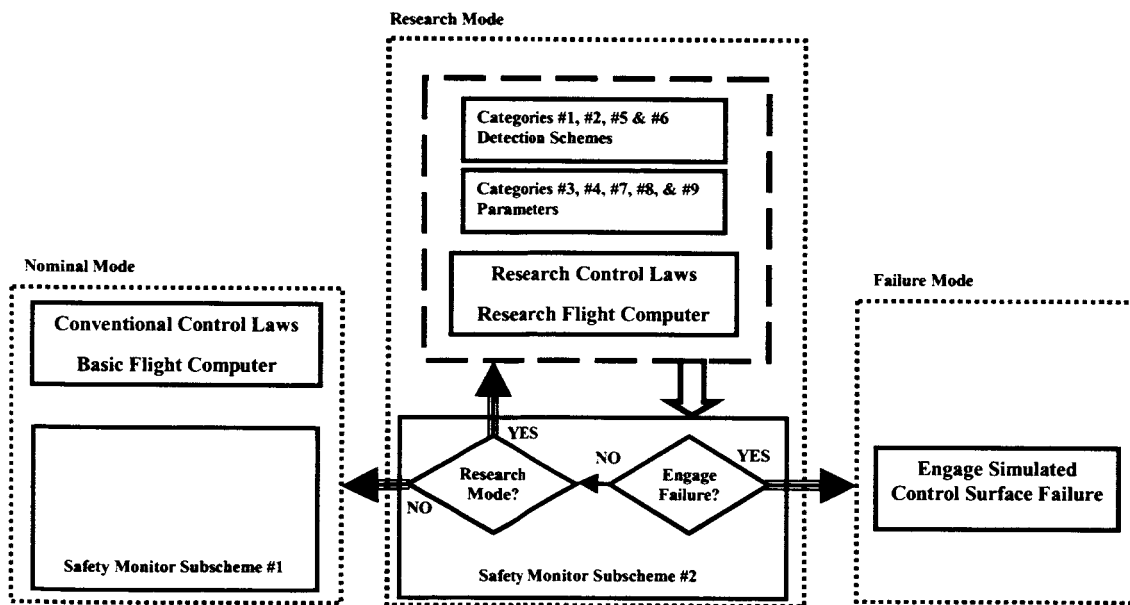


Figure 8. Block Diagram of the Safety Monitor Scheme #2 (SM#2) in Research Mode

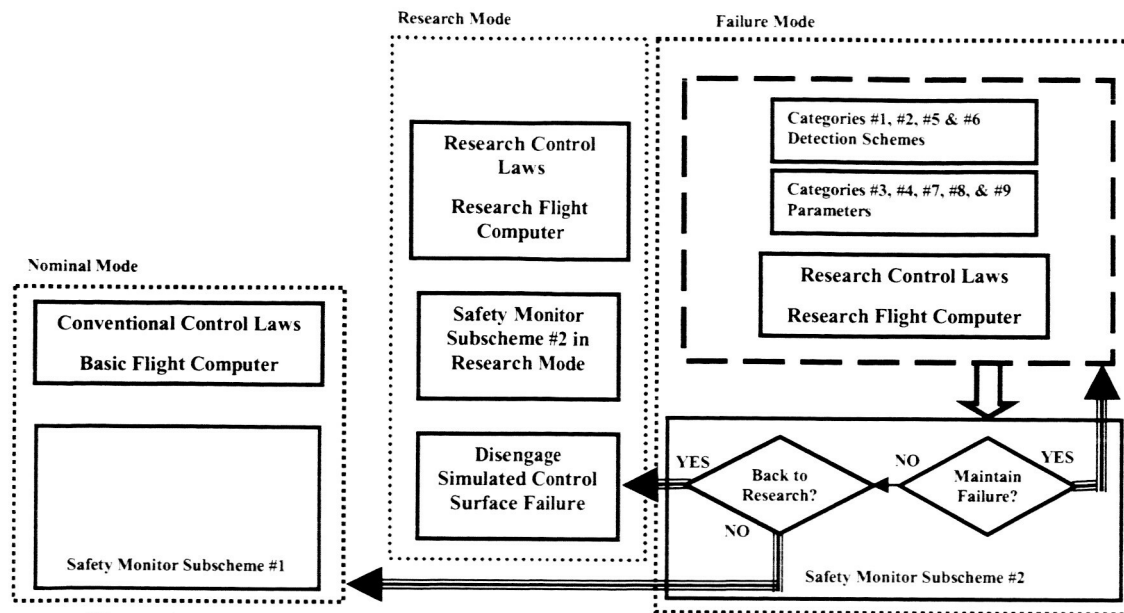


Figure 9. Block Diagram of the Safety Monitor Scheme #2 (SM#2) in Simulated Failure Mode

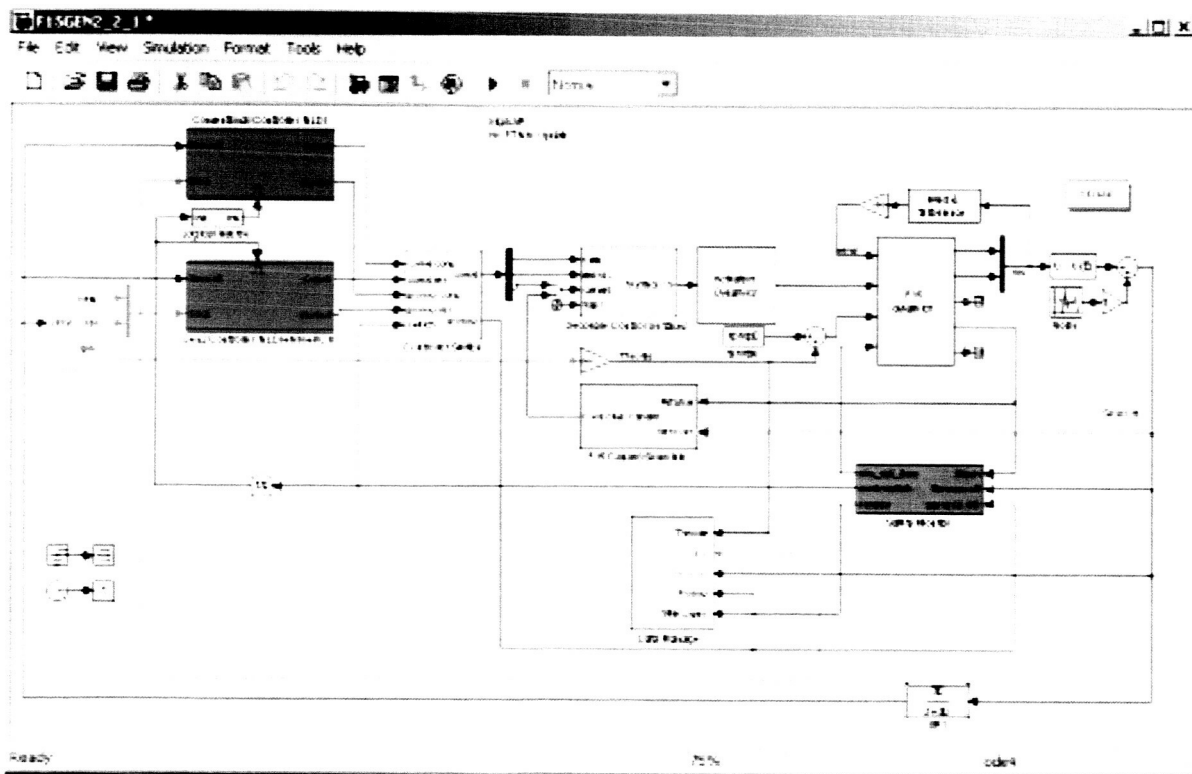


Figure 10. Simulink Scheme of the IFCS F15 Simulation Code

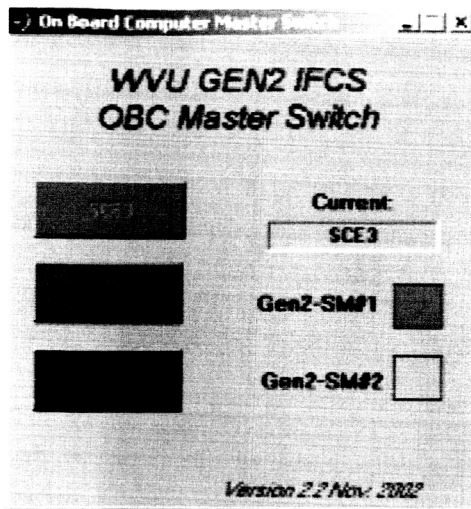


Figure 11. On Board Computer Master Switch

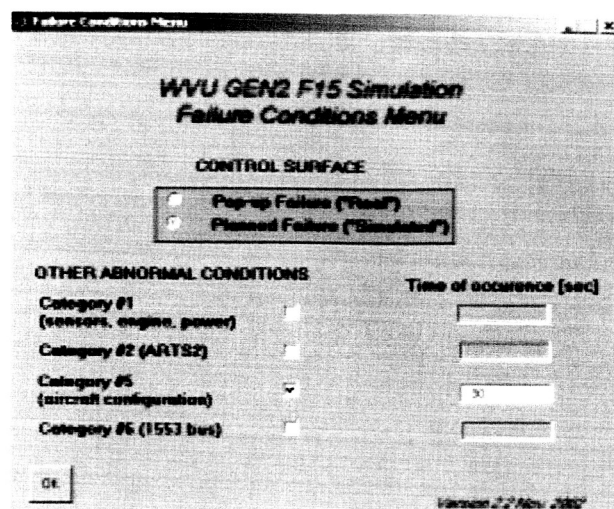


Figure 12. Failure Conditions Menu

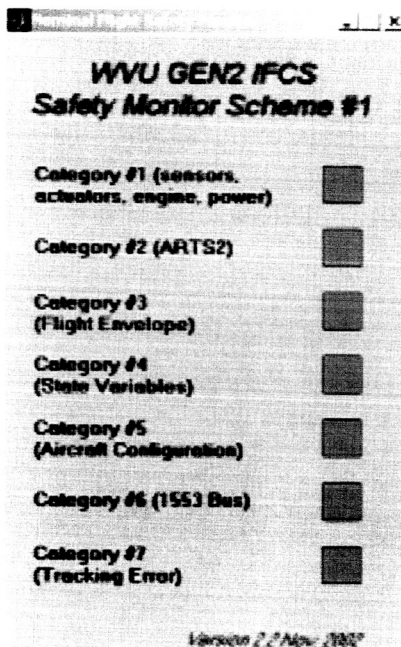


Figure 13. Abnormal Situations - Category Flags for SM#1

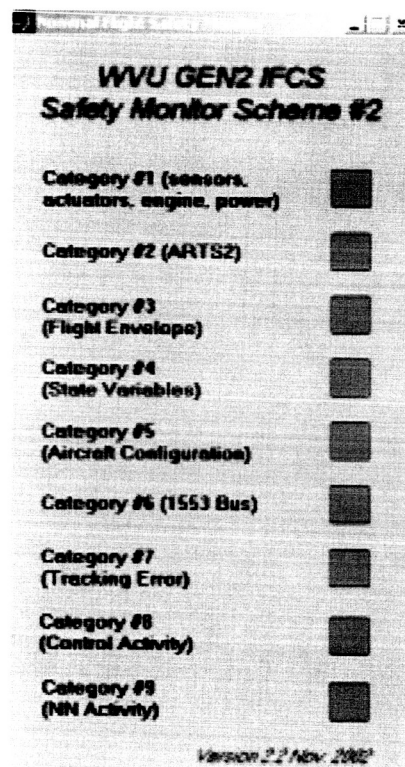


Figure 14. Abnormal Situations - Category Flags for SM#2

WVU GEN2 F15 Simulation
Floating Limiter Menu

Bound = Average +F- Factor x STD +F- Bias

NOMINAL CONDITIONS

	Tracking Error	Control Activity	NN Activity
Failure Based Factor			
Cautionary Based Factor			
Bias			

POST FAILURE TRANSIENT (10 seconds)

	Tracking Error	Control Activity	NN Activity
Failure Based Factor			
Cautionary Based Factor			
Bias			

OK

Version 2.7 Nov. 2007

Figure 15. Floating Limiter Parameters

WVU GEN2 F15 Simulation
Safety Monitor Parameters Visualization Menu

Tracking Error	Control Activity	NN Activity
<input checked="" type="checkbox"/> Roll Rate	<input type="checkbox"/> Left Stabilizer	<input type="checkbox"/> Roll NN Weight: Sum
<input checked="" type="checkbox"/> Pitch Rate	<input type="checkbox"/> Right Stabilizer	<input type="checkbox"/> Roll NN Weight: Sum
<input type="checkbox"/> Yaw Rate	<input type="checkbox"/> Left Control	<input type="checkbox"/> Roll NN Weight: Update Sum
<input type="checkbox"/> Category BT Flag	<input type="checkbox"/> Right Control	<input type="checkbox"/> Roll NN Weight: Update Sum
	<input type="checkbox"/> Left Aileron	<input type="checkbox"/> Roll NN Output
	<input type="checkbox"/> Right Aileron	<input type="checkbox"/> Roll NN Output
	<input type="checkbox"/> Left Rudder	<input type="checkbox"/> Roll NN Output
	<input type="checkbox"/> Right Rudder	<input type="checkbox"/> Roll NN Output
	<input type="checkbox"/> Category RDB Flag	<input type="checkbox"/> Roll NN Output
		<input type="checkbox"/> Category RDB Flag

OK

Version 2.7 Nov. 2007

Figure 16. Safety Monitor Visualization Menu

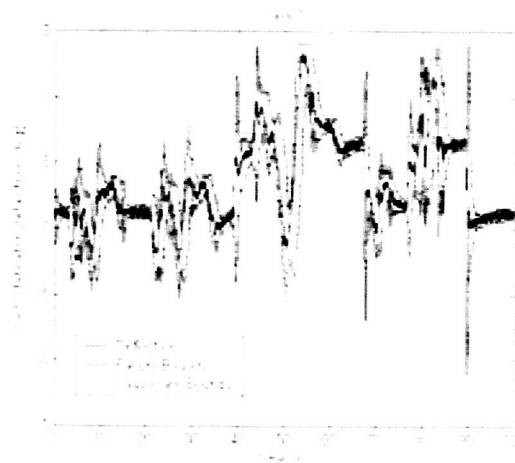


Figure 17. Time Histories of Left Stabilator Deflection Along with Variable Cautionary and Failure Limits – Case #1

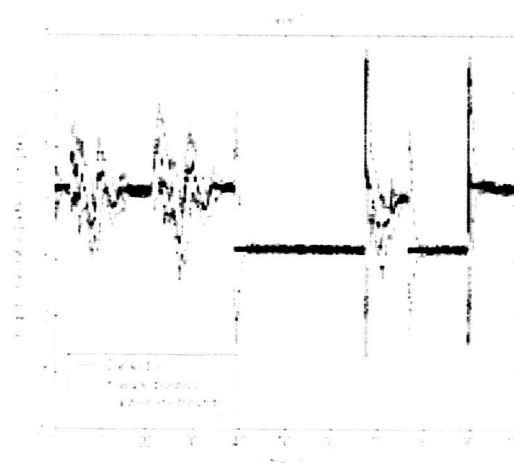


Figure 18. Time Histories of Right Stabilator Deflection Along with Variable Cautionary and Failure Limits - Case 1

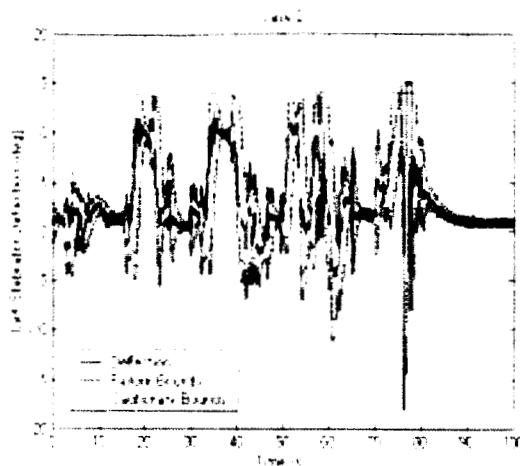


Figure 19. Time Histories of Left Stabilator Deflection Along with Variable Cautionary and Failure Limits - Case 2

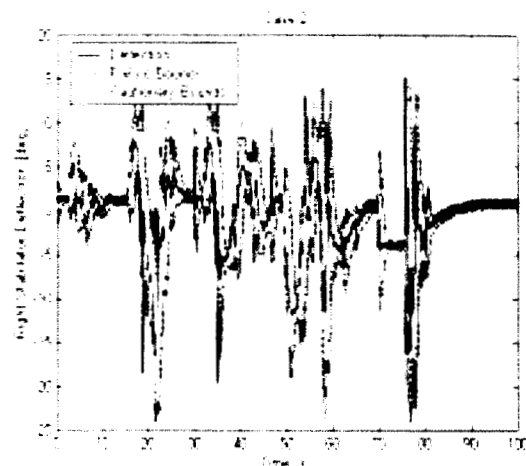


Figure 20. Time Histories of Right Stabilator Deflection Along with Variable Cautionary and Failure Limits - Case 2

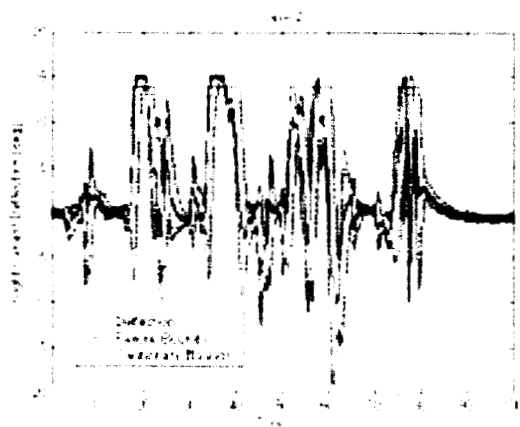


Figure 21. Time Histories of Right Canard Deflection Along with Variable Cautionary and Failure Limits - Case 2

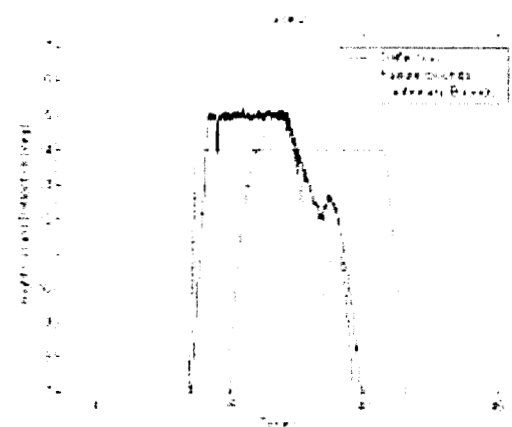


Figure 22. Detail of Right Canard Deflection Time History Showing a category #8 Abnormal Situation - Case 2

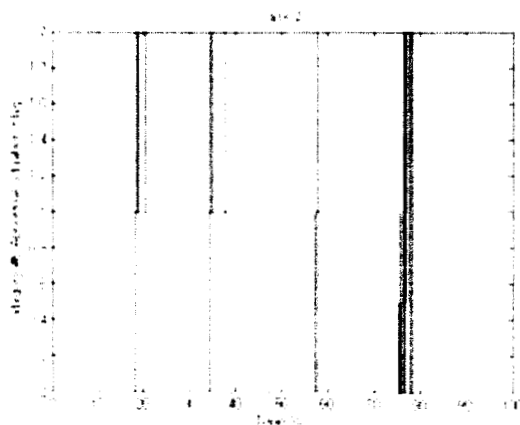


Figure 23. Time History of the Category #8 Flag - Case 2

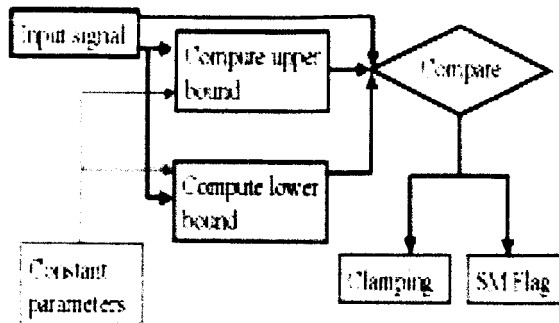


Figure 24. Floating Limiter Logic Block

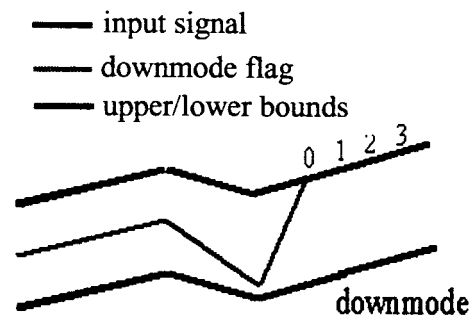


Figure 25. Signal Variation within FL Bounds

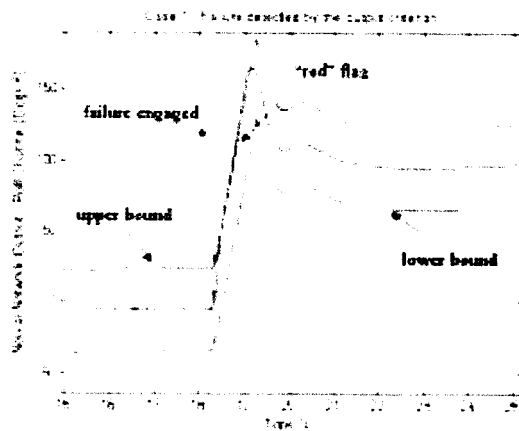


Figure 26. Case #1 - "red" flag due to exceedance of the "NN output" bounds

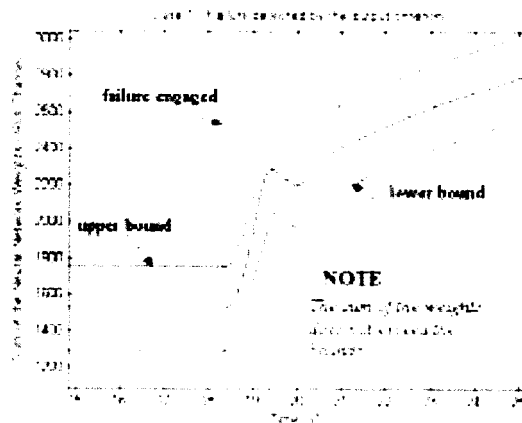


Figure 27. Case #1 - the sum of the weights does not exceed the bounds

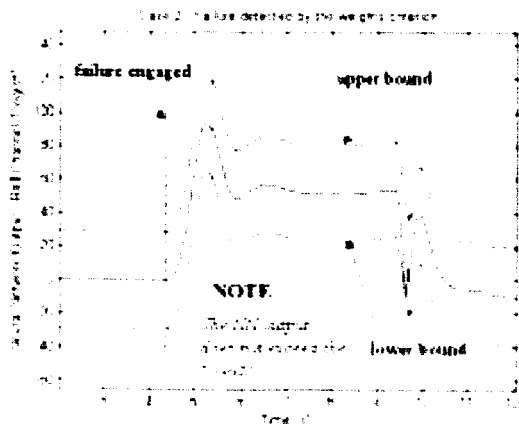


Figure 28. Case #2 - the NN output does not exceed the bounds

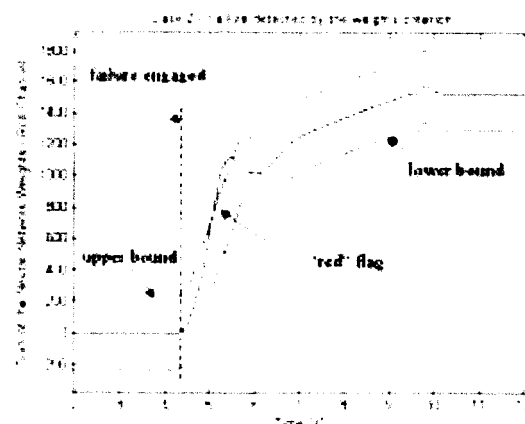


Figure 29. Case #2 - "red" flag due to exceedance of the "NN weights" bounds

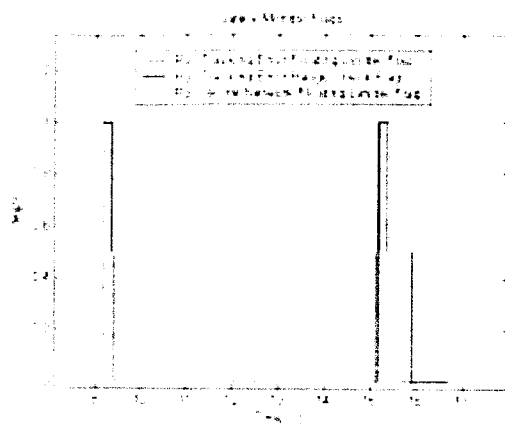


Figure 30. Safety Monitor Flags Roll Rate Tracking Error

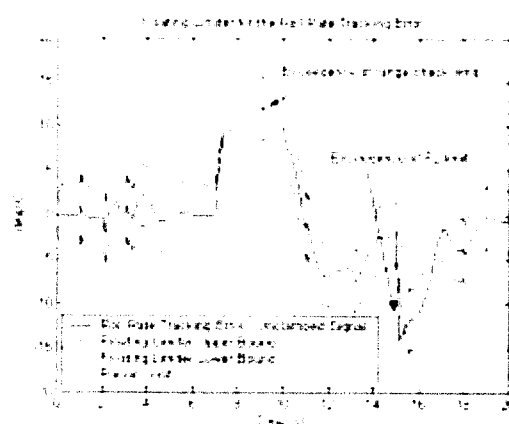


Figure 31. Floating Limiter and Range Check for the Roll Rate Tracking Error

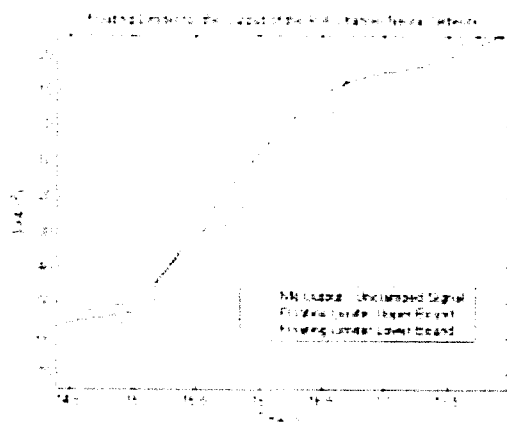


Figure 32. Floating Limiter for the Neural Roll Channel

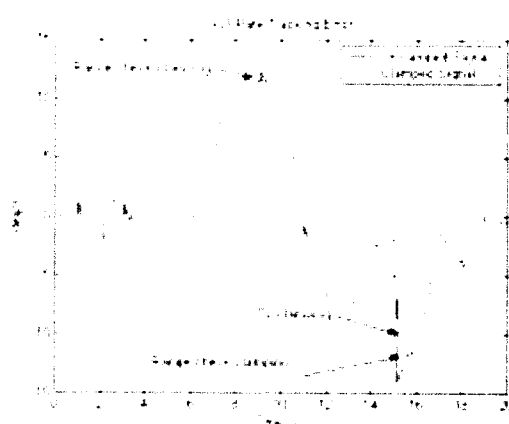


Figure 33. Clamping of the Roll Rate Network Output on the Tracking Error

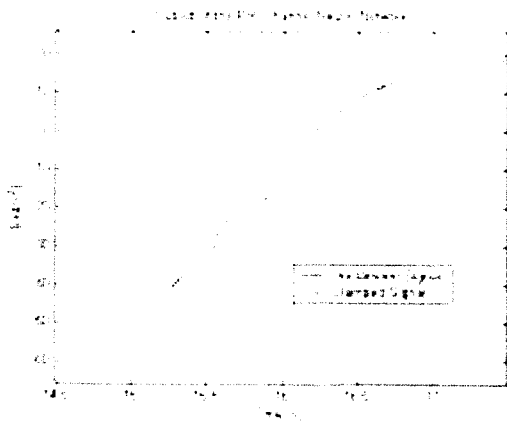


Figure 34. Clamping of the Neural Network Output on the Roll Channel

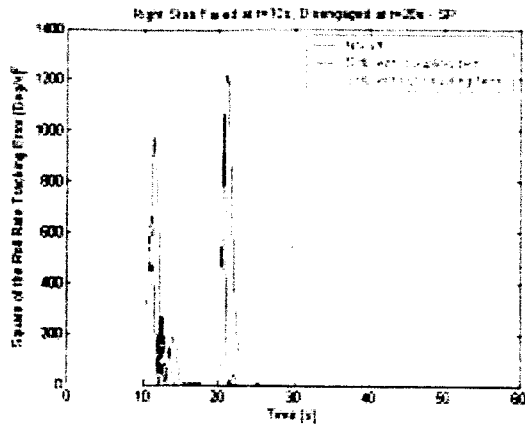


Figure 35. Effect of CCT on the Tracking Error - Roll Channel - Case #1

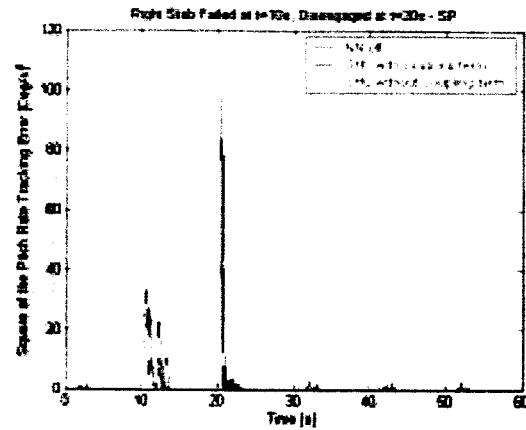


Figure 36. Effect of CCT on the Tracking Error - Pitch Channel - Case #1

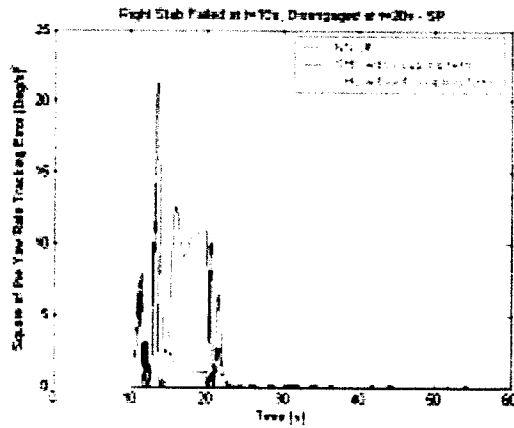


Figure 37. Effect of CCT on the Tracking Error - Yaw Channel - Case #1

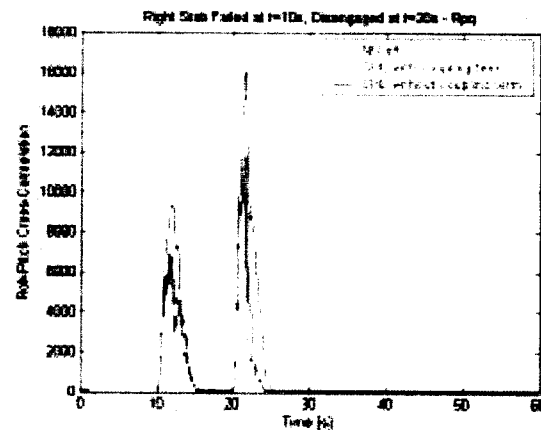


Figure 38. Effect of CCT on the Roll-Pitch Cross-Correlation - Case #1

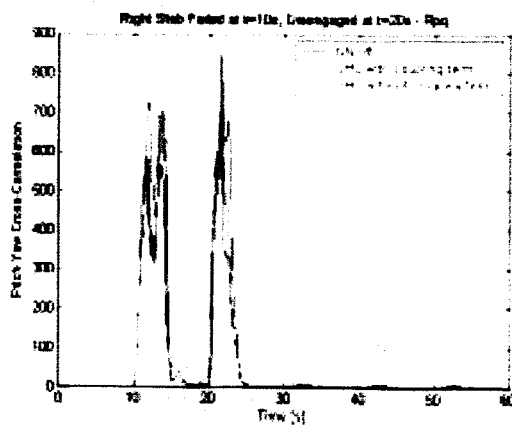


Figure 39. Effect of CCT on the Pitch-Yaw Cross-Correlation - Case #1

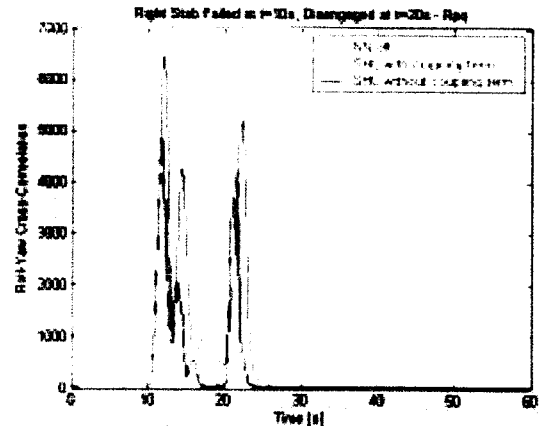


Figure 40. Effect of CCT on the Roll-Yaw Cross-Correlation - Case #1

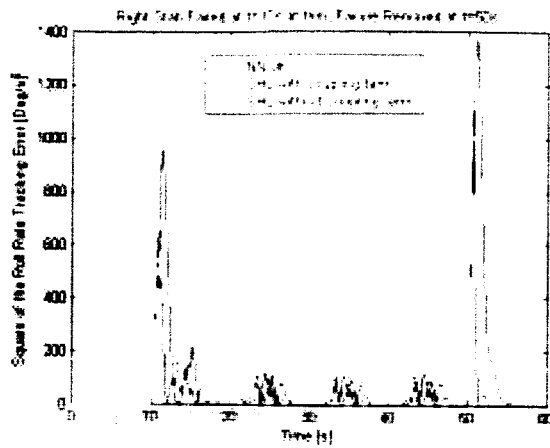


Figure 41. Effect of CCT on the Tracking Error - Roll Channel - Case #2

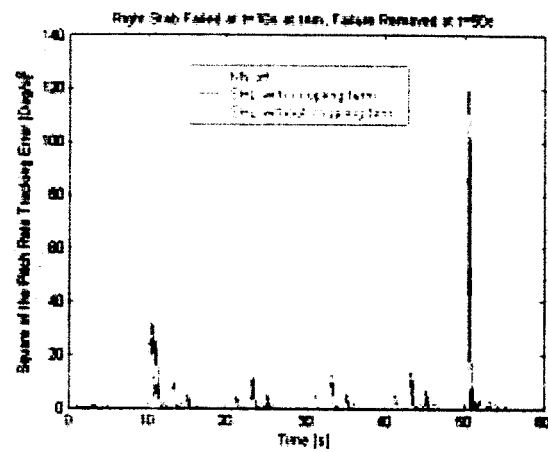


Figure 42. Effect of CCT on the Tracking Error - Pitch Channel - Case #2

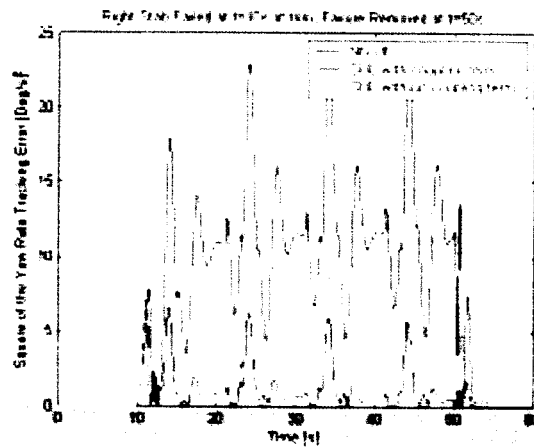


Figure 43. Effect of CCT on the Tracking Error - Yaw Channel - Case #2

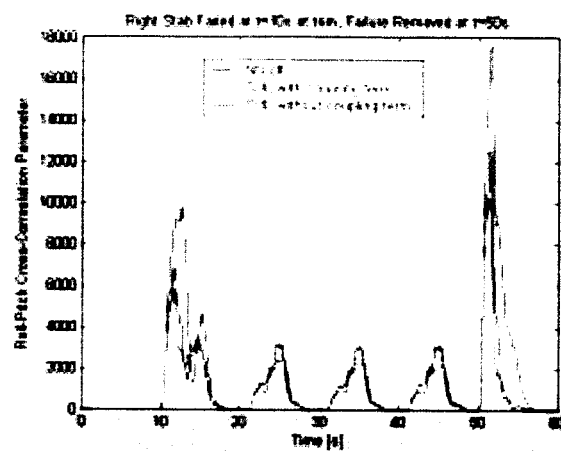


Figure 44. Effect of CCT on the Roll-Pitch Cross-Correlation - Case #2

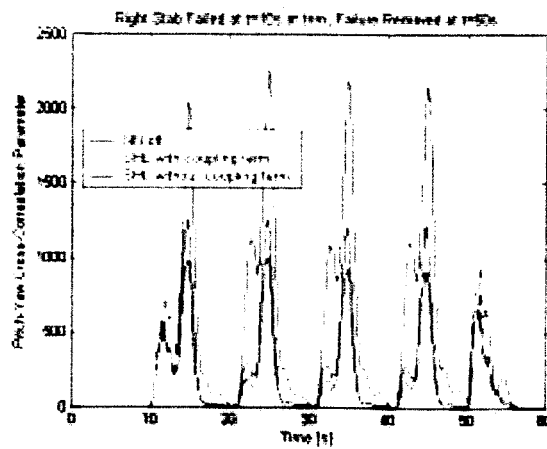


Figure 45. Effect of CCT on the Pitch-Yaw Cross-Correlation - Case #2

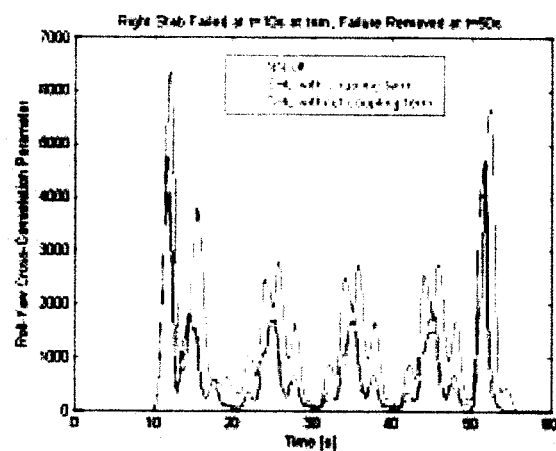


Figure 46. Effect of CCT on the Roll-Yaw Cross-Correlation - Case #2